AGU PUBLICATIONS

JGR

Journal of Geophysical Research: Space Physics

RESEARCH ARTICLE
10.1002/2016JA023591

Key Points:
- MAVEN has observed a transient peak in the Mars ionospheric density profile at an altitude near 200 km
- The second topside density peak is well correlated with the upper ionospheric layer discovered and described by previous studies
- A current sheet associated with the second layer has been discovered

Correspondence to:
A. J. Kopf,
andrew-kopf@uiowa.edu

Citation:
Kopf, A. J., D. A. Gurnett, G. A. DiBraccio, D. D. Morgan, and J. S. Halekas (2017), The transient topside layer and associated current sheet in the ionosphere of Mars, *J. Geophys. Res. Space Physics*, *122*, 5579–5590, doi:10.1002/2016JA023591.

Received 14 OCT 2016
Accepted 24 APR 2017
Accepted article online 26 APR 2017
Published online 9 MAY 2017

The transient topside layer and associated current sheet in the ionosphere of Mars

Andrew J. Kopf[1], Donald A. Gurnett[1], Gina A. DiBraccio[2], David D. Morgan[1], and Jasper S. Halekas[1]

[1]Department of Physics and Astronomy, University of Iowa, Iowa City, Iowa, USA, [2]Solar System Exploration Division, NASA Goddard Space Flight Center, Greenbelt, Maryland, USA

Abstract Radar soundings from the Mars Advanced Radar for Subsurface and Ionosphere Sounding (MARSIS) instrument on board the Mars Express spacecraft have shown that transient layers exist in the dayside upper ionosphere of Mars. The most prominent of these features is a second layer at an altitude near 200 km, well above that of the main photoionization layer. While the general properties of this layer have been studied previously, the inner workings of this layer, and the mechanisms that drive it, are only now becoming clear. With the addition of solar wind, particle, and magnetic field instruments carried by the Mars Atmosphere and Volatile EvolutioN (MAVEN) spacecraft, a more detailed analysis has now been completed. Results show the existence of local current sheets in the upper Martian ionosphere in conjunction with the appearance of the second layer. These currents reveal an important magnetic aspect to the transient layer and point to a variety of possible explanations for its formation, including the Kelvin-Helmholtz instability, magnetic flux ropes, x-type magnetic reconnection, and solar wind magnetic field rotations.

1. Introduction

The Mars Express spacecraft [*Chicarro et al.*, 2004] carries a low-frequency radar called the Mars Advanced Radar for Subsurface and Ionosphere Sounding (MARSIS) that is designed to sound the subsurface and ionosphere of Mars [*Picardi et al.*, 2004]. Prior to MARSIS, radio occultation measurements [*Zhang et al.*, 1990; *Patzold et al.*, 2005] provided most of the knowledge of the Martian ionosphere, along with a pair of profiles measured by the descending Viking landers [*Hanson et al.*, 1977]. Since its deployment in 2005, MARSIS has expanded our understanding of this part of the Martian atmosphere by providing long-term observation, better spatial resolution, and the ability to record measurements in regions where radio occultation cannot be performed.

The first report of the presence of an additional topside ionospheric layer was made by *Gurnett et al.* [2008], which discussed the existence of this transient upper layer, in addition to a more general overview of the ionosphere and its properties. This study revealed that a layer, which we now call the second layer, regularly appeared at an altitude near 200 km. This is well above the 130–140 km altitude of the main photoionization layer, the characteristics of which were well established by *Morgan et al.* [2008]. An example of the appearance of the second layer is shown in Figure 1. Here the ionospheric sounding data are shown as an ionogram, which shows the reflected wave intensity as a function of the transmission frequency and the time delay of the echo. At the maximum plasma frequency of the ionosphere, a cusp appears, symbolizing a maximum in the local density [*Budden*, 1961]. However, as shown in this example, a second cusp often appears at lower frequencies, indicating an additional local maximum in the density profile at a lower density and higher altitude. This "transient layer" was analyzed in great detail by *Kopf et al.* [2008], who confirmed the initial analysis of this feature and conducted a survey of its characteristics, including its altitude, density, and probability of detection. It was additionally reported that further structure may exist even above this layer. However, due to the high-altitude orbit of Mars Express, which has a periapsis altitude near 300 km, no in situ measurements could be made, limiting the ability to conclusively define the structure and origin of the layer.

Starting in late 2014, the Mars Atmosphere and Volatile EvolutioN (MAVEN) spacecraft [*Jakosky et al.*, 2015] began its measurements of the Martian plasma environment. Due to the lower altitude periapsis of MAVEN, which regularly reaches altitudes as low as 150 km, and occasionally as low as 125 km, direct study of this region of the ionosphere is possible on each orbit. MAVEN particle instruments, such as the Neutral Gas and Ion Mass Spectrometer (NGIMS) [*Mahaffey et al.*, 2014] and the SupraThermal and Thermal Ion

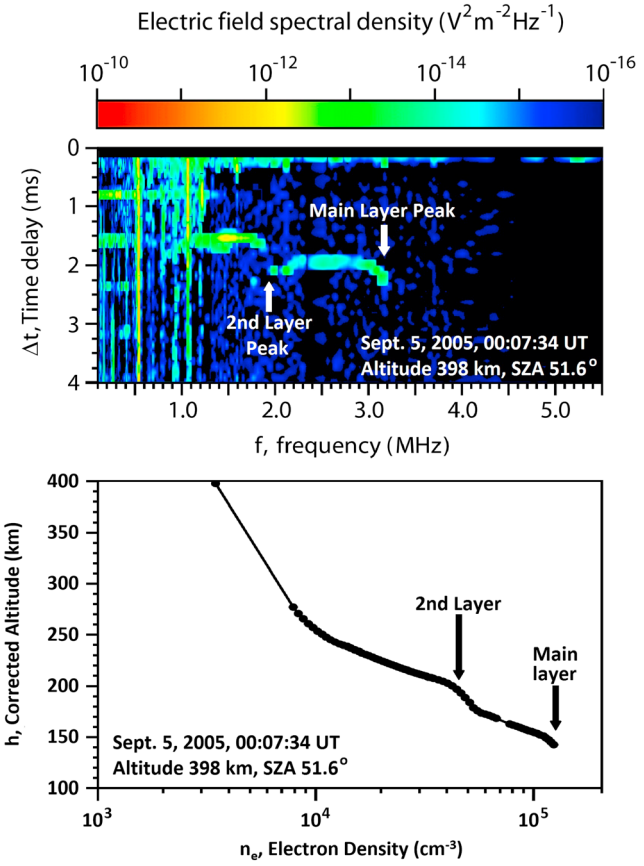

Figure 1. (top) A MARSIS spectrogram, plotting time delay of the received ionospheric echo against frequency, color coded for intensity. Here two cusps appear in the ionospheric echo, indicating two density maximums. As one is at a significantly lower frequency, it is therefore located at an altitude well above the peak of the main ionospheric layer. While not all cusps are this pronounced, their presence is a frequent feature in MARSIS spectrograms. (bottom) The corresponding density profile is also shown. A clear slope change can be seen in the profile at a density near 4×10^4 cm^{-3}. As MARSIS is a topside sounder, it cannot directly observe any cutback in the profile that would show this as a distinct layer, but one can be inferred from the slopes of the measured data points.

Composition (STATIC) instrument [*McFadden et al.*, 2015], can measure the density and velocity of multiple individual ion species and thereby analyze any localized density enhancements in this region. Additionally, the Langmuir Prove and Waves (LPW) instrument [*Andersson et al.*, 2015] can measure the ionospheric electron density, temperature, and the electric field wave excited by the Martian plasma environment. Early results from MAVEN have shown the presence of a localized ion layer [*Bougher et al.*, 2015] at an altitude consistent with the second layer discovered by MARSIS. Large variations in the density profile at this altitude were also reported by *Ergun et al.* [2015], consistent with the transient nature of this region. Furthermore, when MAVEN is outside of the bow shock, instruments such as the Solar Wind Ion Analyzer [*Halekas et al.*, 2015] can measure various solar wind parameters, such as density, temperature, and three-component velocity, at up to about 4 s cadences, which is high enough resolution to correlate with MARSIS observations of this transient feature.

In this paper, we will present new observations of the second layer from both Mars Express and MAVEN, in an effort to gain a more comprehensive understanding of the layer's properties and the mechanism that drives it. In section 2, we discuss the requirements to utilize both spacecraft in near simultaneous observation and the early results in this endeavor. In section 3, we detail the MAVEN-focused broader study, with new insights into the inner structure of the second layer, most notably its magnetic structure. Finally, in section 4, we present multiple mechanisms that may produce the observed layer, focusing on the new magnetic nature that has been observed.

2. Correlated Observations

Before entering into the primary analysis of this paper, we felt it important to include and highlight a special case from more recent data, due to its direct relation to this study. Since Mars Express and MAVEN orbit at different inclinations, their orbital paths will cross twice per orbit, potentially allowing for dual-spacecraft correlated observations of the ionosphere. However, since the two spacecraft orbit with different periods, not every orbit will allow for a useful measurement to be made. Specifically, we refer to the useful orbits for this analysis as the "crossing orbits," defined as orbits where the projected paths of the two spacecraft intersect nearly simultaneously at low altitudes. Put another way, these orbits are those where the two spacecraft fly over (or through) the same point in the Martian ionosphere within a matter of minutes of each other.

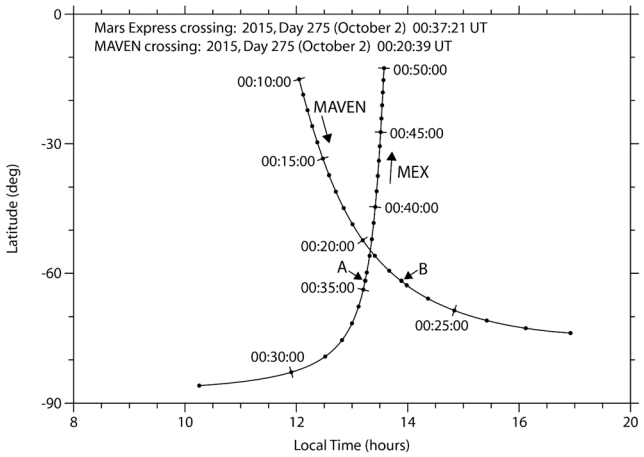

Figure 2. A diagram of the trajectories of Mars Express and MAVEN during the successful crossing orbit observation on 2 October 2015. The dots on the orbital paths mark each minute of the orbit, in UTC. The crossing point can be seen near the center of the image, when Mars Express remotely observed the ionosphere 17 min after MAVEN flew through the same region. MARSIS detected a second cusp in the ionospheric reflection at the time corresponding to point A, about 2 min prior to reaching the orbital crossing point, which aligns well with the peak in the density near 200 km that was measured by NGIMS at point B only 13 min earlier, 2 min after MAVEN has passed the crossing point.

In order to identify these crossing orbits, a series of restrictive criteria were imposed. First, since MARSIS largely only detects the ionosphere on or near the dayside of Mars, due to the significantly lower density on the nightside, the orbits of the two spacecraft were required to cross on the dayside of the planet. Second, MAVEN had to be in the ionosphere, at an altitude less than 400 km, with Mars Express passing overhead at the time of the crossing. Since MAVEN measures ion densities in situ, any cases where measurements were taken at higher altitudes would produce no meaningful result in terms of ionospheric features near the crossing point, and even crossing orbits at this altitude would be difficult to compare. On the other hand, since the MARSIS instrument aboard Mars Express sounds the ionosphere remotely, no altitude restriction is required of Mars Express. However, the ionospheric profiles observed by MARSIS are more precise when studied at lower altitudes, so points near the Mars Express periapsis are still highly preferable.

A third important criterion was that the relevant instruments aboard both spacecraft had to be operating in the correct mode during the crossing orbit. Despite its simplicity, this condition proved highly limiting. The MARSIS instrument is time shared between the Active Ionospheric Sounding mode, which is used to observe the ionosphere, and its Subsurface Sounding mode [*Picardi et al.*, 2004]. Furthermore, due to power limitations, periods of the Mars Express orbit where it is eclipsed by Mars result in the instrument frequently being turned off. Such an event occurred during most of the second potential crossing orbit period in late 2015. For MAVEN, the NGIMS instrument, which is the primary particle instrument used in this investigation, only makes ion measurements on every other orbit, which further limited the number of useful crossings.

Despite these limitations, one set of crossing orbits has proven particularly fruitful in correlating the observations of the two spacecraft. On 2 October 2015, the two spacecraft observed nearly the same area of the ionosphere only 13 min apart, very near a crossing point of the two orbits. The orbital paths of the two spacecraft are shown in Figure 2, which plots the latitude against local time. The time each spacecraft reaches the crossing point is indicated at the top. It can be seen from this diagram that this crossing event occurs in the deep southern hemisphere, shortly after local noon. The two spacecraft measurements were taken only 2 min away from this point, shown in Figure 2 as points A and B, where B marks the time that MAVEN observed the transient second peak in the density and A represents the Mars Express observation time at equivalent latitude where Mars Express identified the same feature.

The measurements obtained during these correlated observations are shown in Figure 3. Figure 3 (top) shows remote sounding measurements from MARSIS, which reveal the presence of the second layer by way of a sharp change in the slope of the ionospheric echo at 1.7 MHz. Likewise, Figure 3 (bottom) displays the electron density profile determined from in situ observations by the NGIMS and LPW instruments, where charge neutrality is assumed for NGIMS so that the electron density is the sum of the densities of the individual ion species. This profile contains a prominent peak in the density at 00:22:45 UTC, when MAVEN is at an altitude of about 190 km. The density of this peak matches well with the 3.6×10^4 cm^{-3} computed from the MARSIS profile. Additional smaller structure can also be seen in this region, but it is unclear whether this is real fine structure or simply instrumental fluctuations in the data. This local density peak is well above the main

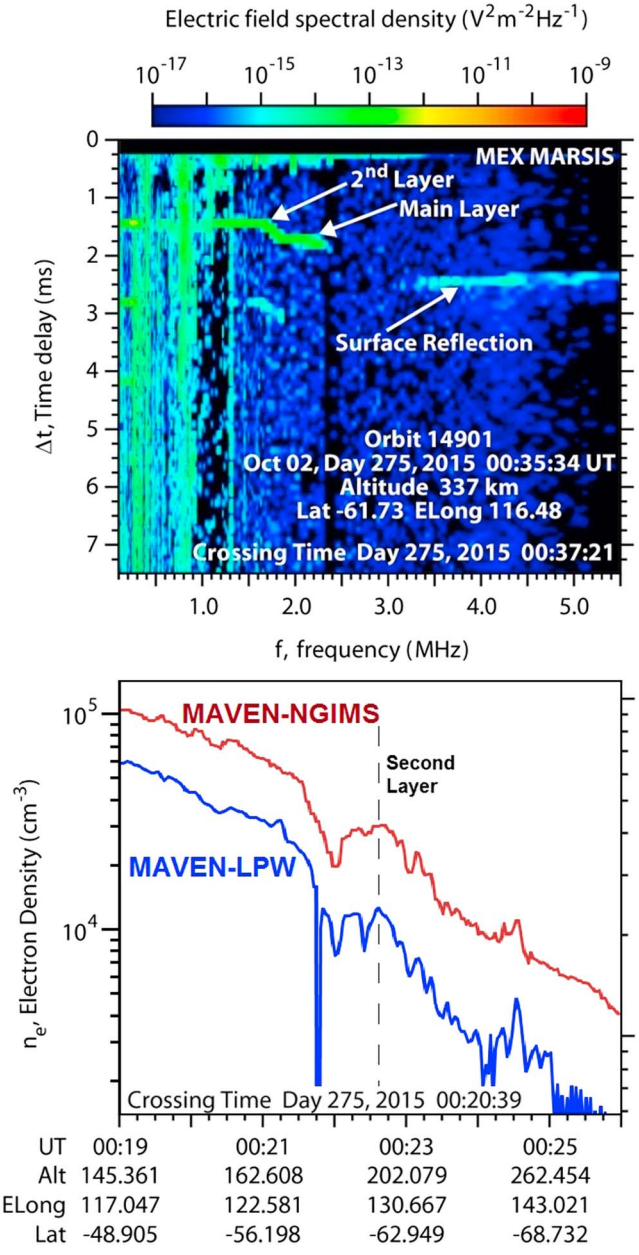

Figure 3. The above figure shows a special case of near-simultaneous observations of a density feature in the ionosphere, only 2 min off the orbital crossing time. (top) The ionospheric echo observed by MARSIS, which shows a remote detection of an interesting transient second layer in the upper ionosphere. (bottom) The density profiles obtained by MAVEN's NGIMS and LPW instruments show a direct in situ detection of this second layer when MAVEN is at the corresponding areographic position. This is the first example of dual-spacecraft detection of a common layer appearance and places some constraints on the stability of the transient second layer.

ionospheric peak, which MAVEN approached at its periapsis altitude of 145 km at 0:18:20 UTC, outside the time range of the figure. The altitude range is consistent with the second layer previously studied through MARSIS observations [*Kopf et al.*, 2008]. This orbit is the first time that two spacecraft have observed the same transient upper layer at Mars and emphatically shows the power of the near-simultaneous spacecraft observation. It also confirms the MARSIS-inspired interpretation that there is a second layer in the ionosphere, defined by a peak in the density profile near 200 km.

3. Features of the Second Layer

As noted above, the addition of MAVEN to the Martian environment has allowed for multispacecraft studies that were until now impossible to accomplish. Since MAVEN's orbit dips to altitudes well below the 200 km region where this feature is observed, the opportunity now exists for in situ measurements of the ions at this altitude. Analysis of the NGIMS data indeed often reveals the presence of a density enhancement at or near 200 km, which as in the crossing orbit case is a result of an increase in the density of virtually all ion species but dominated by O_2^+ ions. An example of this is shown in Figure 4, which displays the densities of all the major ions in the Martian ionosphere, along with their summed total density, during the inbound segment of MAVEN's orbit. The region where the layer appears, at around 2:02 UTC, is dominated by O_2^+ ions by about an order of magnitude, but the layer is seen to be composed of an enhancement in nearly all ion species. The one exception to this density increase of O^+, which shows a slight bump, but overall continues to decline steadily as MAVEN reaches lower altitudes.

To further demonstrate that this feature is the same one routinely observed by MARSIS, a portion of the analysis performed by *Kopf et al.* [2008] was repeated, specifically tracking the altitude at which these features appear with respect to the solar zenith angle. Although detections by MAVEN are limited, due to the brief fly-through nature of the observation, the layer was observed 106 times in the first four MAVEN data

releases (through 15 November 2015), enough to generate meaningful statistics. A map of the MAVEN coverage in the relevant altitude range (170–220 km) during this period is shown in Figure 5. Figure 5 (top) explores the solar zenith coverage at various latitudes. While some solar zenith angles have somewhat more dense coverage than others, the full range from near subsolar to the terminator is explored in the time range of this study. Figure 5 (bottom) displays the geographic distribution, which is largely well covered except for the polar regions. The colored dots have been overlaid onto the coverage map to indicate locations where the second layer was detected in MAVEN observations. Additionally, contours in Figure 5 (bottom) mark the locations of the crustal magnetic fields. While several of the layer detections occur near these crustal fields, many do not, and no clear trend is apparent in their locations.

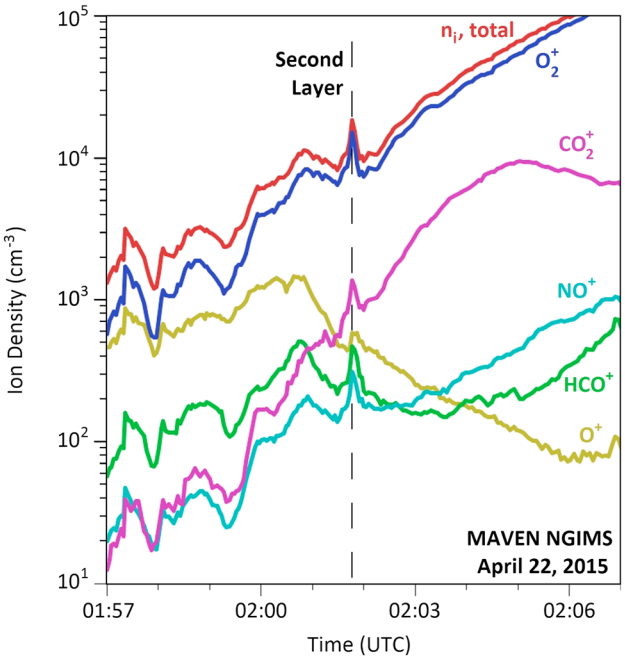

Figure 4. The densities of all major ion species during one detection of the second layer, along with the total ion density, represented by the red line. The layer can be identified by the sharp enhancement in the density just before 02:02 UTC and is marked by the dashed line. The layer is primarily composed of the major ion at this altitude, O_2^+, by an order of magnitude. However, the enhancement can be seen in all major ion species, except perhaps O^+, which increases slightly but inconsistently with the changes in the other ion species.

These cases were identified by examining the NGIMS ionospheric density profile above 170 km, where the ionosphere is out of photochemical equilibrium. Although MAVEN has multiple instruments capable of making density measurements, we elected to use NGIMS as the primary particle instrument for this investigation. This choice was made primarily because of the ability of NGIMS to measure not only the total local density but also the density of many individual ion species, which allowed the composition of the layer to be studied. The LPW data were then used as a double check on the NGIMS measurements. The observations for each orbit were studied by eye to locate these density enhancements. For each possible detection, only localized increases in the density by at least 30% were considered to be the second layer to reduce the likelihood of instrument fluctuations affecting the results. Additionally, only the lowest altitude case that would be visible to a topside sounder like MARSIS was used, as *Kopf et al.* [2008] noted the occasional presence of additional lower density structure above the second topside layer.

The colored dots in Figure 5 represent the locations where the second layer was observed, and analysis of their altitude distribution is shown in Figure 6. Here the MAVEN-observed altitudes of this layer are plotted against solar zenith angle in 10° bins, similar to what was previously done by *Kopf et al.* [2008] with MARSIS observations. As the MAVEN orbit does not provide completely uniform coverage, the number of events in each bin varies. It is quickly apparent that this result is consistent with that previous study, which found the average altitude of the layer to be between 190 and 200 km for most solar zenith angles. Additionally, analysis of the detection frequency shows a trend with solar zenith angle, as the layer was observed by NGIMS near 40% of the time on the dayside of Mars, but only about 10% near the terminator. Both of these results are roughly consistent with the 2008 study. Combined with the crossing orbit discussed in section 2, this gives a high degree of confidence that the MAVEN-observed density peak is the same feature that was detected and analyzed in the previous study by *Kopf et al.* [2008].

There is the larger question of why the density enhancement exists in the first place. To help understand this, results from the magnetometer (MAG) aboard MAVEN [*Connerney et al.*, 2015] were added to the overall

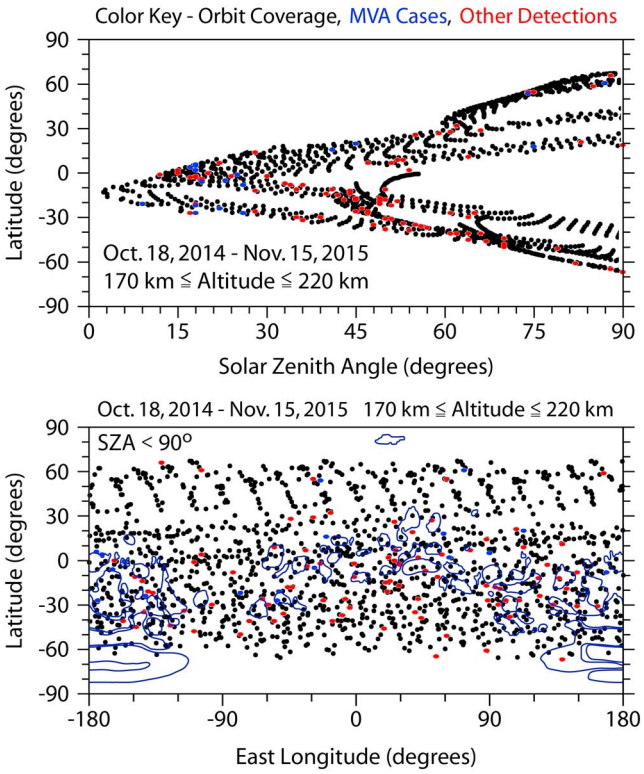

Figure 5. (top and bottom) MAVEN orbital coverage for the 6 month period of this study, computed from the spacecraft ephemeris data, restricted to only the relevant altitudes of 170–220 km. The black dots represent the overall coverage and are computed in 5 min intervals, so each orbit will be represented by no more than a few dots for both the inbound and outbound segments. The colored dots represent layer detections, with the blue marking those that underwent minimum variance analysis to study their associated current, and the red indicating all other detections during this time period. Contours overlaid in Figure 5 (bottom) map contours of the Mars crustal magnetic field.

analysis. In doing so, it revealed that the enhancement in the density was accompanied in about 85% of these cases by a localized minimum in the overall magnetic field strength at the same altitude, coincident with a rotation in one or more of the magnetic field components. Two representative layer detections are shown in Figures 7 and 8. Figures 7 and 8 (top) show the total electron density measured by the LPW instrument, while Figures 7 and 8 (middle) gives the overall ion density from NGIMS, calculated by a sum of all the individual ion species. In both cases, the spacecraft was increasing in altitude, so density is expected to be decreasing, which it does until about 04:41 UTC in Figure 7 and 09:36 in Figure 8. At these times, a significant density enhancement can be seen around 200 km in altitude. Interestingly, both cases also show a second sharp density increase at higher altitudes in at least one of the density measurements. This large fluctuation is likely connected to the "third layer" noted by *Kopf et al.* [2008] but is beyond the scope of this study. Figures 7 and 8 (bottom) display the magnetic field strength and components obtained from the MAG measurements, shown in Mars-centered Solar Orbital (MSO) coordinates, where x is toward the Sun and z perpendicular to the orbital plane. A 15–20 nT decrease in the overall magnetic field magnitude is seen to coincide roughly with the peak of the density enhancement in Figures 7 and 8 (middle) in both cases. A modeled crustal magnetic field strength is also plotted in both cases. A rotation in the magnetic field, identified by multiple magnetic components changing from a positive orientation to a negative one, or vice versa, indicates the presence of a current in this region.

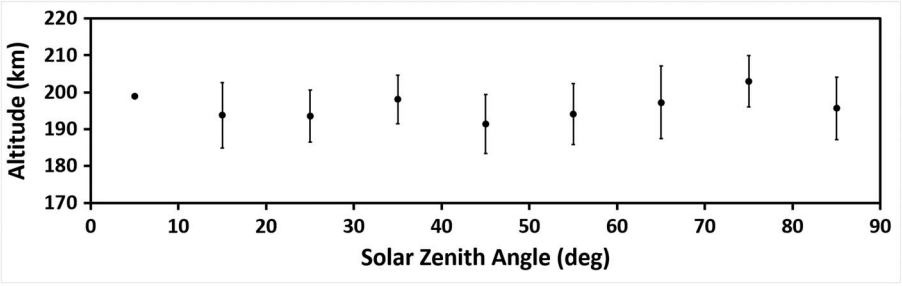

Figure 6. A statistical correlation between the altitude of the upper layers and the solar zenith angle. These MAVEN-observed values, obtained by the NGIMS instrument, include 106 layer detections in the first four MAVEN data releases, sorted into 10° bins. These findings are consistent with the results obtained by *Kopf et al.* [2008], which observed this layer to be generally between 190 and 200 km for most solar zenith angles.

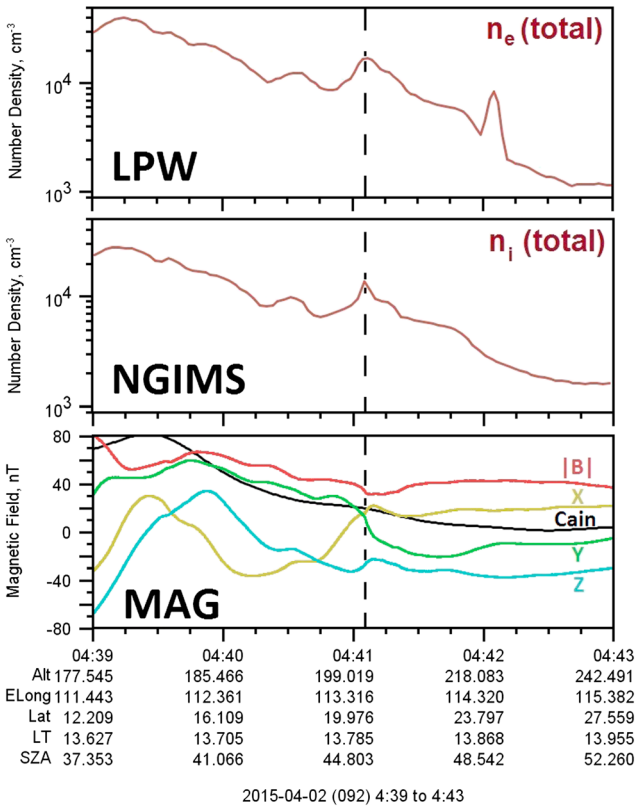

Figure 7. A comparison between measurements of the total electron density obtained by the (top) MAVEN LPW instrument, (middle) total ion density from NGIMS, and (bottom) the local magnetic field from the magnetometer, MAG (bottom). The Cain model crustal magnetic field strength is also plotted in Figure 7 (bottom). The panels are centered on an upper layer observation made during the outbound portion of a MAVEN orbit, marked by the dashed line. As the spacecraft rises in altitude, a sudden sharp increase of the density occurs near 200 km, which is correlated with a significant dip in the magnetic field strength near its peak. This dip is the result of a rotation of multiple magnetic field components and indicates the presence of a current in the ionosphere at that altitude. LPW also displays an additional density increase above 200 km, though this is not reflected in the other two instrument readings.

In order to analyze the nature and orientation of this current, 18 of the detections with more prominent magnetic field variations were selected to undergo minimum variance analysis [*Sonnerup and Cahill*, 1967], in order to identify the normal direction of the current sheet, and therefore its orientation with respect to the planet. These are indicated by the blue dots in Figure 5. Due to the constraints required on the magnetic field in this type of analysis, not all the detected cases could be used, as the less prominent ones would not likely achieve statistical significance when comparing the resulting eigenvectors. Indeed, even one of the 18 provided an unusable result. The remaining events, however, produced some interesting findings. First, and perhaps most significantly, the orientation of the current sheet is highly variable. While a stable layer or boundary region might be expected to produce a horizontally stratified current with respect to the planet's surface, the current sheet associated with this upper layer varies widely in its orientation, ranging from less than 10° to nearly 90° off of horizontal, meaning nearly perpendicular to the surface. Furthermore, there is no direct relation between this orientation and the layer's altitude, solar zenith angle, or latitude. Similarly, when observing the rotated direction of this tilted current sheet, where no rotation is a north-south tilt and a 90° rotation is toward east-west, we also see considerable variability in the current sheet's orientation, with no correlation to the conditions listed above.

There is, however, a possible correlation between the orientation of this current sheet and the local time where the observation was made. A decreasing trend appears between the tilt of the current sheet away from the normal as the spacecraft moves from dawn to dusk, suggesting that the current becomes more horizontally stratified, and therefore perhaps more stable, over the course of increasing daylight hours on Mars (0600–1800 UTC). This trend is shown in Figure 9a, where the local time is plotted against the degree of tilt of the current sheet with respect to horizontal stratification above Mars, forming a near-linear connection between the two variables. While this trend is owed in large part to the two cases with very horizontal current sheets, there is nothing special about those two points that might otherwise skew the result. They are at different solar zenith angles at low northern latitudes, and both appear in regions where the local magnetic field is around 40 nT. Other correlations are also plotted in the other three panels of Figure 9, relating this tilt to solar zenith angle (Figure 9b), altitude (Figure 9c), and latitude (Figure 9d), but the data were not well organized in any of these. Given that the lone apparent dependence is with local time, there is a possible solar connection to the stability of the current, and perhaps to its origin as well.

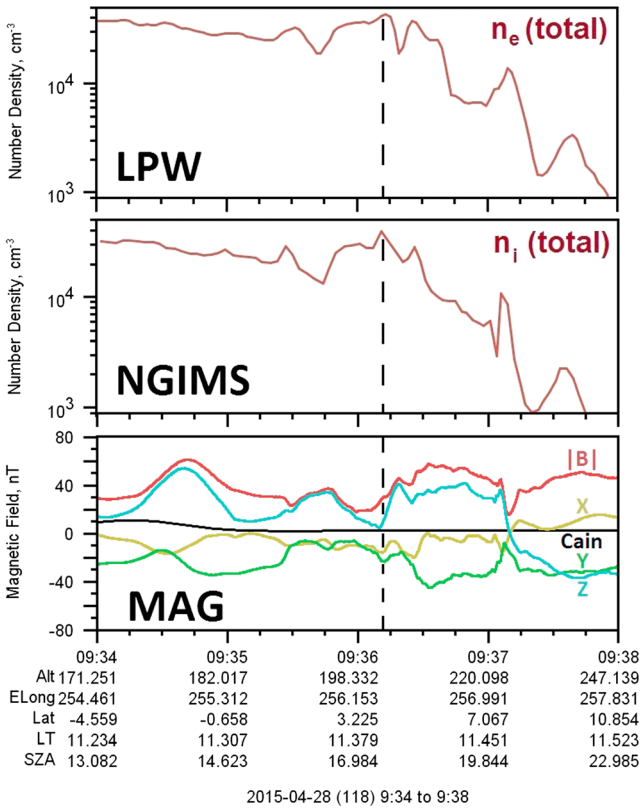

Figure 8. Another example of an upper layer observed by MAVEN. As in Figure 7, the (top) LPW total electron density is plotted against ion density measurements by the (middle) NGIMS instrument and (bottom) magnetic field measurements from MAG, along with the local Cain model magnetic field. The upper layer can be seen just to the right of the center of the time range, indicated by the dashed line, and correlates well with changes in the magnetic field, which occur near the peak in the density profile. All three instruments detect an additional density spike and probable current at near 230 km as well.

One related aspect that was important to consider is the influence of the crustal magnetic fields [*Acuña et al.*, 1998]. This magnetism has been mapped all across the surface of the planet [*Connerney et al.*, 2005], and various spherical harmonic models have been devised to compute its components and strengths [e.g., *Cain et al.*, 2003; *Arkani-Hamed*, 2004]. Although *Kopf et al.* [2008] found no direct correlation between the crustal fields and the detection of the second layer, a result supported by a significantly larger study [*Kim et al.*, 2012], the limited time range and indirect nature of that early study left room for the possibility of a connection on a broader scale.

An analysis in this case tends to be largely consistent with previous findings. It is clear from Figure 5 (bottom) that several of the layer detections are in or near regions of crustal magnetism. However, only 10 of the cases detected by MAVEN are along or reasonably near strong crustal fields of 100 nT or larger. The vast majority of the MAVEN observations are in regions where the field strength is significantly smaller and in some cases virtually nonexistent. On average, the layer appears in a region where the crustal field strength is less than 50 nT, about one third of the average peak strength during each orbit. When neglecting the 10 cases of higher magnetic field strength, the average drops even further to about 30 nT. It should be considered, though, that the crustal fields may still play an indirect role, as their location (dayside, nightside, or terminator) can have global effects on ionospheric structures [e.g., *Andrews et al.*, 2015; *Dubinin et al.*, 2016; *Withers et al.*, 2005]. Finally, one interesting detail of note is that the observation of the layer was generally on the polewardside of the main magnetic features present during the orbital pass. It is unclear at this point whether this is a real feature or due to selection bias, but if it is indeed real, it would suggest some sort of role for the crustal fields in the layer's generation.

4. Possible Explanations

We have considered several possibilities for the origin of this second topside layer. One long-postulated explanation for the formation of this layer has been a plasma instability, most likely the Kelvin-Helmholtz instability. This process occurs where a velocity shear exists between two fluids or plasmas, which in this case could result from an interaction of the ionospheric plasma with the solar wind. Recently, partially developed vortices due to these types of waves have been observed at the sheath-ionospheric boundary at Mars [*Ruhunusiri et al.*, 2016], so it is plausible that this effect could happen in this region as well. However, cases analyzed so far show no conclusive evidence of any such velocity gradient across the layer, and it is unclear why such a velocity shear would exist at this particular altitude of the Martian ionosphere. Furthermore, an analysis of the current sheets present in this region suggests that the currents become more horizontal

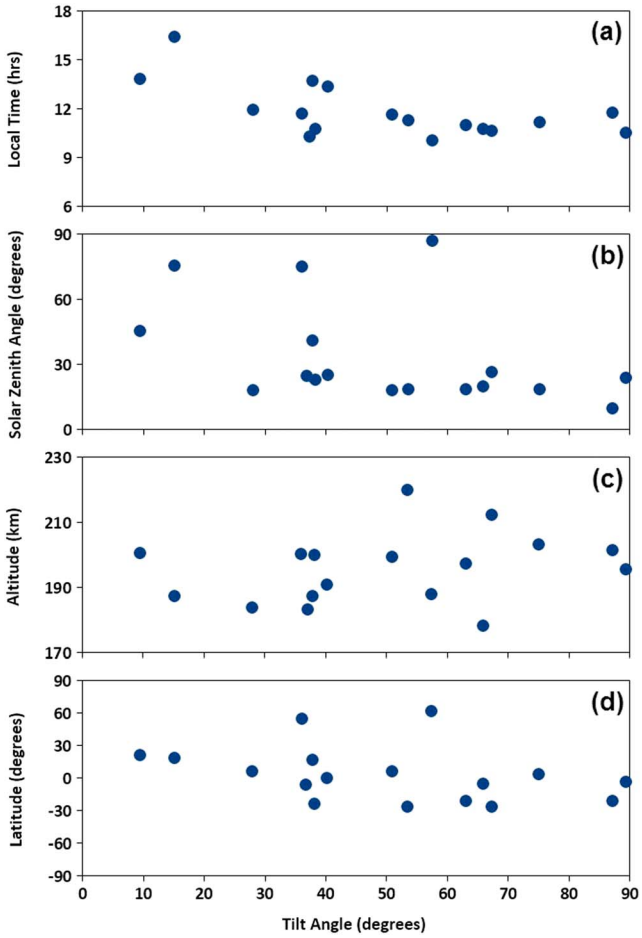

Figure 9. Various spacecraft position parameters plotted against the angle at which the current sheet is tilted with respect to horizontal stratification above Mars. (a) A possible correlation between the local time and the tilt angle, which would suggest a solar connection to the formation of the second layer. The remaining three panels plot (b) solar zenith angle, (c) altitude, and (d) latitude against the tilt angle but are overall not well correlated.

closer to the dusk terminator, contrary to the instability's nature of being more unstable and dynamic at high solar zenith angles.

That observation by itself, however, is not enough to rule out this possibility. The Kelvin-Helmholtz instability has been observed to have a dawn-dusk asymmetry at Mercury [*Sundberg et al.*, 2012], where it was seen to form exclusively in one hemisphere, the duskside in that case. This was suggested to be due to Larmor radius effects. It also has been observed to be asymmetric at Saturn [*Ma et al.*, 2014], again with a preference for the duskside of the ionosphere, despite predictions that it would favor the dawn sector. The reason was less clear in this case, though the most likely explanation is that the fast-growing modes diffused too quickly in the dawn sector but were able to propagate into the dusk sector and grow in different shear flow conditions. Some dawn-dusk asymmetries have been observed at Mars, such as the ability of all major ion species to reach higher altitudes in the dawn sector [*Benna et al.*, 2015]. However, it is currently unknown if a Kelvin-Helmholtz asymmetry exists at Mars, which unlike Mercury and Saturn is largely unmagnetized, and there is no asymmetry present in the upper layer detections from this study. Furthermore, the wave nature of the Kelvin-Helmholtz instability allows for the possibility that MAVEN could observe this current at a variety of different orientations at the same instability vortex, depending solely on its position as it reaches this altitude. While the current would be horizontal near the peak of the vortex, it could appear more angled away from that position. The variety of orientations observed in the survey of the magnetic currents performed above could simply be a consequence of how close MAVEN flew to any particular peak. These considerations support the Kelvin-Helmholtz instability as a viable possibility for the formation of this layer, but it remains unclear why they would be generated at this altitude in the dayside ionosphere.

Another option considered for the layer's origin was that of magnetic flux ropes. Flux ropes have been commonly observed at Mars [e.g., *Briggs et al.*, 2011], so their appearance here would not be a surprising phenomenon. However, a few of their standard characteristics did not fit the observed features of this layer. First and foremost was the behavior of the magnetic field. While a clear rotation is consistently observed as MAVEN flies through this region, which would be expected with a flux rope, an axial magnetic field should also be present, which would appear as an increase in the magnetic field magnitude, coincident with the inflection of the field rotation. However, MAG generally observes a sharp decrease in the magnitude instead. Furthermore, the minimum variance analysis that was performed should have yielded a minimum magnetic field eigenvector with a magnitude close to zero if MAVEN was crossing near the center of a flux rope structure, which was consistently not the case. Finally, the size of these structures is significantly smaller than other

flux ropes observed at Mars. Density profiles have shown the second layer to be no more than a few tens of kilometers thick, and generally even smaller, significantly less than the flux ropes seen elsewhere at Mars, which range from many tens to hundreds of kilometers in size. These considerations suggest that flux ropes are unlikely to be the solution here.

One related explanation that addresses many of these problems is that these layers are "crater" flux ropes [*Farrugia et al.*, 1988]. While a flux rope contains a well-defined core magnetic field due to being compressed by the surrounding twisted magnetic field, a crater flux rope lacks this magnetic configuration. This is because the compression by the curvature force is counteracted by enhanced plasma pressure at the core of the flux rope, potentially leading to a local minimum of the magnetic field [*Ding et al.*, 1991]. These aspects fix many of the problems of the more general flux rope explanation detailed above. Interestingly, it has been suggested that crater flux ropes are the initial stages of more typical flux ropes [*Zhang et al.*, 2010]. That may also explain the lack of a discernable plasma flow across this region.

Another possibility is that the transient layer could be generated by x-type magnetic reconnection. Indeed, a few of the characteristic signatures of this process are regularly present in the observations. First, the magnetized nature of this layer, regardless of the location on the planet (i.e., crustal field influence), implies a local magnetic interaction in the upper ionosphere. Additionally, the rotation in the magnetic field signature, a characteristic feature indicating the presence of a current sheet, is also an expected characteristic of reconnection. If reconnection is indeed the cause of this transient layer, then it is in reality more of a localized phenomenon than an actual layer. However, a current sheet alone does not directly imply reconnection, and it is unclear what processes would drive it at this altitude to form this layer, especially given the layer's tendency for appearing away from crustal magnetic field features [*Kim et al.*, 2012].

One key missing characteristic of reconnection is that of a detectable plasma flow. In x-type magnetic reconnection, the plasma should be ejected at the Alfvén velocity following the reconnection event. In this region of the ionosphere, the Alfvén velocity is on the order of 1–2 km/s. While this should be within the sensitivity of the STATIC instrument [*McFadden et al.*, 2015], no discernable plasma flow has been detected in the cases studied. The absence of a plasma flow would also seemingly rule out other related explanations, such as plasma clouds [*Halekas et al.*, 2016] or vertical plasma transport in general.

Still, this missing element cannot be considered conclusive proof against reconnection and similar mechanisms. STATIC is only able to observe within a limited angular field, the angle of which depends on which mode the instrument is in. If this flow were in a direction outside of this range, it could elude the instrument's detection. Furthermore, events of magnetic reconnection in the near-Mars magnetotail were found to exhibit counterstreaming beams, with bulk velocities varying by ion species [*Harada et al.*, 2015]. If this model of species-dependent velocity holds true in the ionosphere, this type of magnetic reconnection may be difficult to observe at these lower altitudes.

One potential explanation for the absence of significant plasma flow associated with reconnection may be the geographic location of these layers. The initial results reported by *Kopf et al.* [2008] noted that these layers appeared all over the planet, including in the significantly less magnetized northern hemisphere. More recently it was demonstrated that the layer was almost exclusively present away from the main magnetism regions in the Southern Hemisphere, and especially common in the low-magnetism regions [*Kim et al.*, 2012], a finding backed up by this study, which found the bulk of these layer detections to be in the Northern Hemisphere or near the equator, with less than a handful anywhere near the strong southern crustal field regions. This finding combined with those by *Harada et al.* [2015] makes it possible that these are magnetized plasma parcels downstream from a more subsolar reconnection point. The reasonably high-density plasma environment would cause a decrease in the plasma flow velocity, as it propagated through this region, and explain the transient nature of these events, as these parcels would likely evolve on fairly short time scales in this medium. Furthermore, this model would also account for the decreasing detectability with increasing solar zenith angle, as these plasma parcels would become increasingly incoherent over time.

One final option for the formation of a current layer may lie in the magnetic field convection. As the solar wind travels through space, it carries with it a magnetic field. However, when it reaches an obstacle, in this case Mars, these magnetic fields will pile up and try to work their way around the planet. It is well established that the plasma flow velocity is slowed significantly inside the bow shock of Mars [*Duru et al.*, 2010], with

magnetic field pileup occurring on the dayside inside of that boundary [*Trotignon et al.*, 2006; *Dubinin et al.*, 2007]. As a result, not only will the solar wind plasma be slowed as it flows around Mars but so will the magnetic fields carried within its flow. The consequence of this is a draping of the magnetic field and may result in a magnetic memory effect in the Martian ionosphere, not unlike the phenomenon seen at Titan [*Bertucci et al.*, 2008].

As all of this happens, there will be instances where two regions with different magnetic field orientation will come into contact with each other, resulting in the formation of a current layer between them. This feature is dependent upon changes in the solar wind clock angle. In the MSO coordinate system, the clock angle is defined as the angle in the *y-z* plane between the *z* axis and the magnetic field carried by the solar wind. Therefore, its appearance will be transient and will be most prevalent near the subsolar point, not toward the limbs of the planet. Since Mars Express is in a polar orbit, it would frequently cross these draped field lines as it traverses the dayside of the planet. The combination of these effects could explain the transient behavior of these upper layer features, with the current features tied to the upstream magnetic field variations in the solar wind.

All of this matches with the primary characteristics of this transient upper layer. However, this model would suggest that the current layer would likely be horizontally stratified, due to the geometry of its formation, which is not consistent with our analysis. In fact, as noted previously, the current has instead been seen in some cases to be oriented near vertically, which is difficult to rectify with this interpretation. Furthermore, an analysis of the interplanetary magnetic field (IMF) orientations on the inbound and outbound segments of these orbits was inconclusive at best, revealed no clear consistent differences in the magnetic field orientations or solar wind parameters. This is in direct conflict with this model's method of forming a current layer, unless the IMF orientation can rotate multiple times on a time scale shorter than the period where MAVEN is in the ionosphere. As MAVEN cannot measure the solar wind while in the ionosphere, such rotations would not be directly detected. More generally, it is also not clear that the magnetic field in the solar wind can rotate regularly enough, and on short enough time scales, to account for the MARSIS observations presented by *Kopf et al.* [2008], as the layer was seen to appear multiple times over the course of a single 40 min sounding pass. These considerations make this model increasingly unlikely.

Acknowledgments
The MARSIS investigation at the University of Iowa was supported by NASA through contract 1224107 with the Jet Propulsion Laboratory. G.A.D. was supported by a NASA Postdoctoral Program appointment at the Goddard Space Flight Center, administered by Universities Space Research Association (USRA) through a contract with NASA. MARSIS data are available through the Geosciences Node of NASA's Planetary Data System (PDS) at http://pds-geosciences.wustl.edu. MAVEN data are available via the Planetary Plasma Interactions node of the PDS at http://ppi.pds.nasa.gov. Finally, we also wish to thank Majd Mayyasi and Mehdi Benna of the MAVEN team for fruitful discussions related to this research.

References

Acuña, M. H., et al. (1998), Magnetic field and plasma observations at Mars: Initial results of the Mars Global Surveyor mission, *Science*, *279*(5357), 1676–1680, doi:10.1126/science.279.5357.1676.

Andersson, L., et al. (2015), The Langmuir Probe and Waves (LPW) instrument for MAVEN, *Space Sci. Rev.*, *195*(1), 173–198, doi:10.1007/s11214-015-0194-3.

Andrews, D. J., N. J. T. Edberg, A. I. Eriksson, D. A. Gurnett, D. Morgan, F. Němec, and H. J. Opgenoorth (2015), Control of the topside Martian ionosphere by crustal magnetic fields, *J. Geophys. Res. Space Physics*, *120*, 3042–3058, doi:10.1002/2014JA020703.

Arkani-Hamed, J. (2004), A coherent model of the crustal magnetic field of Mars, *J. Geophys. Res.*, *109*, E09005, doi:10.1029/2004JE002265.

Benna, M., P. R. Mahaffey, J. M. Grebowsky, J. L. Fox, R. V. Yelle, and B. M. Jakosky (2015), First measurements of the composition and dynamics of the Martian ionosphere by MAVEN's Neutral Gas and Ion Mass Spectrometer, *Geophys. Res. Lett.*, *42*, 8958–8965, doi:10.1002/2015GL066146.

Bertucci, C., et al. (2008), The magnetic memory of Titan's ionized atmosphere, *Science*, *321*(5895), 1475–1478, doi:10.1126/science.1159780.

Bougher, S., et al. (2015), Early MAVEN Deep Dip campaign reveals thermosphere and ionosphere variability, *Science*, *350*, doi:10.1126/science.aad0459.

Briggs, J. A., D. A. Brain, M. L. Cartwright, J. P. Eastwood, and J. S. Halekas (2011), A statistical study of flux ropes in the Martian magnetosphere, *Planet. Space Sci.*, *59*, 1498–1505, doi:10.1016/j.pss.2011.06.010.

Budden, K. G. (1961), *Radio Waves in the Ionosphere*, pp. 160–162 , Cambridge Univ. Press, Cambridge, U. K.

Cain, J. C., B. B. Ferguson, and D. Mozzoni (2003), An $n = 90$ internal potential function of the Martian crustal magnetic field, *J. Geophys. Res.*, *108*(E2), 5008, doi:10.1029/2000JE001487.

Chicarro, A., P. Martin, and R. Traunter (2004), The Mars Express mission: An overview, in *Mars Express: The Scientific Payload*, edited by A. Wilson, SP-1240, pp. 3–16, Eur. Space Agency Publ. Div., Noordwijk, Netherlands.

Connerney, J. E. P., et al. (2005), Tectonic implications of Mars crustal magnetism, *Proc. Natl. Acad. Sci.*, *102*, 14970–14975, doi:10.1073/pnas.0507469102.

Connerney, J. E. P., et al. (2015), The MAVEN magnetic field investigation, *Space Sci. Rev.*, *195*(1), 257–291, doi:10.1007/s11214-015-0169-4.

Ding, D.-Q., L.-C. Lee, and Z.-W. Ma (1991), Different FTE signatures generated by the bursty single X line reconnection and the multiple X line reconnection at the dayside magnetospause, *J. Geophys. Res.*, *96*, 57–66, doi:10.1029/90JA01989.

Dubinin, E., et al. (2007), Plasma morphology at Mars. ASPERA-3 observations, *Space Sci. Rev.*, *126*(1), 209–238, doi:10.1007/s11214-006-9039-4.

Dubinin, E., M. Fraenz, D. Andrews, and D. Morgan (2016), Martian ionospher observed by Mars Express. 1. Influence of the crustal magnetic fields, *Planet. Space Sci.*, *124*, 62–75, doi:10.1016/j.pss.2016.02.004.

Duru, F., D. A. Gurnett, J. D. Winningham, R. Frahm, and R. Modolo (2010), A plasma flow velocity boundary at Mars from the disappearance of electron plasma oscillations, *Icarus*, *206*(1), 74–82, doi:10.1016/j.icarus.2009.04.012.

Ergun, R. E., M. W. Morooka, L. A. Andersson, C. M. Fowler, G. T. Delory, D. J. Andrews, A. I. Eriksson, T. McEnulty, and B. M. Jakosky (2015), Dayside electron temperature and density profiles at Mars: First results from the MAVEN Langmuir probe and waves instrument, *Geophys. Res. Lett.*, *42*, 8846–8853, doi:10.1002/2015GL065280.

Farrugia, C. J., R. P. Rijnbeek, M. A. Saunders, D. J. Southwood, D. J. Rodgers, M. F. Smith, C. P. Chaloner, D. S. Hall, P. J. Christiansen, and L. J. C. Woolliscroft (1988), A multi-instrument study of flux transfer event structure, *J. Geophys. Res.*, *93*, 14,465–14,477, doi:10.1029/JA093iA12p14465.

Gurnett, D. A., et al. (2008), An overview of radar soundings of the Martian ionosphere from the Mars Express spacecraft, *Adv. Space Res.*, *41*, 1335–1346, doi:10.1016/j.asr.2007.01.062.

Halekas, J. S., et al. (2015), The Solar Wind Ion Analyzer for MAVEN, *Space Sci. Rev.*, *195*(1), 125–151, doi:10.1007/s11214-013-0029-z.

Halekas, J. S., et al. (2016), Plasma clouds and snowplows: Bulk plasma escape from Mars observed by MAVEN, *Geophys. Res. Lett.*, *43*, 1426–1434, doi:10.1002/2016GL067752.

Hanson, W. B., S. Sanatani, and D. R. Zuccaro (1977), The Martian ionosphere as observed by the Viking retarding potential analyzers, *J. Geophys. Res.*, *82*, 4351–4363, doi:10.1029/JS082i028p04351.

Harada, Y., et al. (2015), Magnetic reconnection in the near-Mars magnetotail: MAVEN observations, *Geophys. Res. Lett.*, *42*, 8838–8845, doi:10.1002/2015GL065004.

Jakosky, B. M., et al. (2015), The Mars Atmosphere and Volatile Evolution (MAVEN) mission, *Space Sci. Rev.*, *195*(1), 3–48, doi:10.1007/s11214-015-0139-x.

Kim, E., et al. (2012), The analysis of the topside additional layer of Martian ionosphere using MARSIS/Mars Express data, *J. Astron. Space Sci.*, *29*(4), 337–342, doi:10.5140/JASS.2012.29.4.337.

Kopf, A. J., D. A. Gurnett, D. D. Morgan, and D. L. Kirchner (2008), Transient layers in the topside ionosphere of Mars, *Geophys. Res. Lett.*, *35*, L17102, doi:10.1029/2008GL034948.

Ma, X., B. Stauffer, P. A. Delamere, and A. Otto (2014), Asymmetric Kelvin-Helmholtz propagation at Saturn's dayside magnetopause, *J. Geophys. Res. Space Physics*, *120*, 1867–1875, doi:10.1002/2014JA020746.

Mahaffey, P. R., et al. (2014), The Neutral Gas and Ion Mass Spectrometer on the Mars Atmosphere and Volatile Evolution mission, *Space Sci. Rev.*, *195*(1), 49–73, doi:10.1007/s11214-014-0091-1.

McFadden, J. P., et al. (2015), MAVEN SupraThermal and Thermal Ion Composition (STATIC) instrument, *Space Sci. Rev.*, *195*, 199–256, doi:10.1007/s11214-015-0175-6.

Morgan, D. D., D. A. Gurnett, D. L. Kirchner, J. L. Fox, E. Nielsen, and J. J. Plaut (2008), Variation of the Martian ionospheric electron density from Mars Express radar soundings, *J. Geophys. Res.*, *113*, A09303, doi:10.1029/2008JA013313.

Patzold, M., S. Tellmann, B. Hausler, D. Hinson, R. Schaa, and G. L. Tyler (2005), A sporadic third layer in the ionosphere of Mars, *Science*, *310*, 837–839.

Picardi, G., et al. (2004), MARSIS: Mars Advanced Radar for Subsurface and Ionosphere Sounding, in *Mars Express: The Scientific Payload*, edited by A. Wilson, *Eur. Space Agency Spec. Publ.*, SP-1240, 51–70.

Ruhunusiri, S., et al. (2016), MAVEN observations of partially developed Kelvin-Helmholtz vortices at Mars, *Geophys. Res. Lett.*, *43*, 4763–4773, doi:10.1002/2016GL068926.

Sonnerup, B. U. O., and L. J. Cahill (1967), Magnetopause structure and attitude from Explorer 12 observations, *J. Geophys. Res.*, *72*(1), 171–183, doi:10.1029/JZ072i001p00171.

Sundberg, T., S. A. Boardsen, J. A. Slavin, B. J. Anderson, H. Korth, T. H. Zurbuchen, J. M. Raines, and S. C. Solomon (2012), MESSENGER orbital observations of large-amplitude Kelvin-Helmholtz waves at Mercury's magnetopause, *J. Geophys. Res.*, *117*, A04216, doi:10.1029/2011JA017268.

Trotignon, J. G., C. Mazelle, C. Bertucci, and M. H. Acuña (2006), Martian shock and magnetic pile-up boundary positions and shapes determined from the Phobos 2 and Mars Global Surveyor data sets, *Planet. Space Sci.*, *54*, 357–369, doi:10.1016/j.pss.2006.01.003.

Withers, P., M. J. Mendillo, H. Rishbeth, D. P. Hinson, and J. Arkani-Hamed (2005), Ionospheric characteristics above Martian crustal magnetic anomalies, *Geophys. Res. Lett.*, *32*, L16204, doi:10.1029/2005GL023483.

Zhang, M. G. H., J. G. Luhman, A. J. Kliore, and J. Kim (1990), A post-Pioneer Venus reassessment of the Martian dayside ionosphere as observed by radio occultation methods, *J. Geophys. Res.*, *95*, 14,829–14,839, doi:10.1029/JB095iB09p14829.

Zhang, H., et al. (2010), Evidence that crater flux transfer events are initial stages of typical flux transfer events, *J. Geophys. Res.*, *115*, A08229, doi:10.1029/2009JA015013.